Science and Engineering of Composite Materials 14, 271-297 (2007)

The Effect of Varying the In-plane Loads and Stacking Sequence on the Vibration Analysis of Composite Stiffened Plates

Sung-Cheon Han [a,*], Samuel Choi [b], Weon-Tae Park [c]

[a] *Department of Civil Engineering, Daewon Science College, 599 Shinwol, Jecheon, 390-702, Korea*
[b] *Division of Structural Engineering, EO Engineers Co. Ltd, Anyang, 431-060, Korea*
[c] *Department of Civil Engineering, Kongju National University, 275 Budai, Cheonan, 330-717, Korea*

ABSTRACT

The natural frequencies and mode shapes of composite stiffened plates with stiffener are presented by using the assumed natural strain 9-node shell element. To compare with previous research, the stiffened plates are composed of carbon-epoxy composite laminate with a symmetric stacking sequence. Also, the result of the present shell model for the stiffener made of composite materials is compared with that of the beam model. In the case of torsionally weak stiffener, a local buckling occurs in the stiffener. In this case, the stiffener should be idealized by using the shell elements. The current investigation concentrates upon the vibration analysis of rectangular stiffened and un-stiffened composite plates when subjected to the combination of in-plane compressive and shear loads. The in-plane compressive and shear loads affect the natural frequencies and mode shapes of the stiffened laminated composite plates. As a result of the increase in the in-plane compressive load and the variation of fiber angle of skin plate, the sequence of some of the mode shapes are interchanged. This implies that the present shell model for the stiffened plate produces more accurate results. Therefore, to obtain the correct vibration mode, the stiffeners are modeled as a shell element. To solve the eigenvalue problems, the Lanczos method is employed.

Keywords: B. Vibration; C. Laminates; Composite stiffened plates; Assumed natural strain

1. INTRODUCTION

The wide applications of the laminated composite plates in the civil, aerospace, marine and other industries have found their advantages of high stiffness to weight ratio, high strength to weight ratio, resistance to corrosion and high damping property in comparison with metal plates. Most structures, whether used in air, sea or on land, are subjected to dynamic loads during their operation. Especially, exposed to a dynamic situation, these materials offer better characteristics than any other conventional materials. The weight saving is an important consideration for high performance applications. Also, for the vibration problem of plates, it is often necessary to minimize the maximum deflections of plates without introducing any considerable weight penalty. This can be achieved by adding stiffeners to the plates.

The study on the free vibration analysis of isotropic plates using a shell element can be found in Lee and Han /1/.

* Corresponding author. Tel.: +82-43-649-3267 ; fax.: +82-43-649-3137
E-mail address : techv11@mail.daewon.ac.kr (Sung-Cheon Han).

The analytical solutions for free vibration of laminated composite plates were discussed in the works of Reddy /2/ and Kant *et al.* /3/. Aydogdu and Timarci /4/ presented vibration analysis of cross-ply laminated plates with twelve different combinations of edge boundary conditions using the Ritz method. Han and Choi /5/ have published static and vibration analysis of laminated composite plates and shells using the lumped mass matrix. Park *et al.* /6/ studied linear static and dynamic analysis of laminated composite plates and shells using a 4-node quasi-conforming shell element. A 3-D analysis using a resultant 8-node solid element was presented by Kim *et al.* /7/.

A number of papers on isotropic stiffened plates have been proposed. Olsen and Hazell /8/ have presented results from a theoretical and experimental comparison study on the vibration characteristics of all clamped and eccentrically stiffened isotropic plates. They used a triangular finite element in the calculations. Mukherjee and Mukhopadhyay /9/ used an 8-node finite element model for vibration analysis. Palani *et al.* /10/ have published performance studies of the two models for static and vibration analysis of stiffened plates with various boundary conditions using four mass lumping schemes. Liu and Chen /11/ investigated the free vibrations of a skew cantilever plate with a stiffener by a finite element method. Recently, Lee *et al.* /12/ presented vibration analysis of laminated composite plates with stiffeners using shell element for the skin plate and beam element for the stiffener. Also, Rikards *et al.* /13/ studied vibration analysis of composite stiffened plates using the beam element for the stiffener. In order to reduce the degree of freedom of assembled structure, they used a beam element in the vibration analysis. But they presented that if the stiffener is flexurally and rotationally stiff and skin of the shell is thin, then the local mode of the skin is dominant. In this case for stiffeners the beam elements can be used. In the case of torsionally weak stiffener, a local buckling occurs in the stiffener. In this case, the stiffener should be idealized by using the shell elements.

In order to overcome the shear locking problems Huang *et al.* /14/ developed a 9-node assumed strain shell element using the enhanced interpolation of the transverse shear strains in the natural coordinate system. Other finite elements employing the assumed strain method were then reported by Jang and Pinsky /15/ independently and also a variational background of the assumed strain method was presented by Simo and Hughes /16/. Belytschko *et al.* /17/ presented a 9-node assumed strain shell element with a stabilized matrix to control the hourglass mode and calculated all the terms by using a reduced integration. In this paper, to avoid locking phenomena, the assumed natural strain method in the shell element by Han *et al.* /18-20/ and Lee and Han /21/ is used. The concept of resultant-stress shell element, which was based on the equivalent natural constitutive equation from an explicit transformation scheme, is used. This concept was extended to the nonlinear analysis in the 8-node finite element works of Kim *et al.* /22/. Attaf and Hollaway /23/ studied vibration analyses of eccentrically stiffened and un-stiffened GRP composite plates subjected to in-plane forces. However, work on the vibration analysis of the stiffened anisotropic plate under the combination of in-plane compression and shear loading has rarely been published.

For this reason, we use the assumed natural strain 9-node shell element and concentrated on the vibration analysis of eccentrically stiffened rectangular composite plates under the circumstances of combining axial compression and shear loading. In this study, first-order shear deformation theory and the resultant shell element concept are used for composite stiffened plates. The analytical solutions are presented to show the application of the shell formulation to rectangular laminated composite plates under free vibration conditions. The Lanczos method is employed in the calculation of the eigenvalues of composite stiffened plates and the Gauss integration rule is adopted to evaluate the mass matrix. The solutions of the vibration analysis are numerically illustrated in a number of figures to show the influence of the types of in-plane loads, the magnitude of in-plane loads and the fiber-angle of skin plate and stiffener.

2. GEOMETRY AND KINEMATICS OF SHELL

The geometry of a 9-noded shell element with six degrees of freedom is shown in Fig. 1.

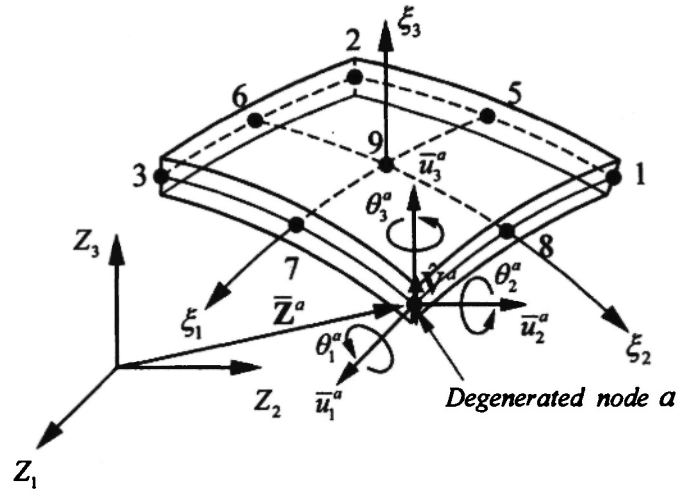

Fig. 1: Geometry of 9-node shell element with six degrees of freedom

Using the shell assumption of straight normal remaining straight, the initial configuration of the shell element having thickness h^a can be written as

$$\mathbf{Z}(\xi_i) = \bar{\mathbf{Z}}(\xi_\beta) + \xi_3 \bar{\mathbf{V}}(\xi_\beta) \; ; \; i = 1,2,3 \; , \; \beta = 1,2 \tag{1}$$

$$\mathbf{Z}(\xi_\beta) = \sum_{a=1}^{9} N_a(\xi_\beta)\bar{\mathbf{Z}}^a \tag{2}$$

$$\bar{\mathbf{V}}(\xi_\beta) = \sum_{a=1}^{9} N_a(\xi_\beta)\frac{h^a}{2}\hat{\mathbf{V}}^a \tag{3}$$

where $\mathbf{Z}$ denotes the position vector of a generic point in the shell element; $\bar{\mathbf{Z}}$ is the position vector of a point in the mid-surface; N_a denotes the two-dimensional quadratic Lagrangian interpolation function associated with node a; $\bar{\mathbf{Z}}^a$ are position vectors which have three Cartesian components; h^a is the thickness of the shell at node a; and $\hat{\mathbf{V}}^a$ is a unit normal vector at node a, which is normal to the mid-surface. The unit normal vector $\hat{\mathbf{V}}^a$ at node a can be easily determined by

$$\hat{\mathbf{V}}^a = \frac{\dfrac{\partial \bar{\mathbf{Z}}^a}{\partial \xi_1} \times \dfrac{\partial \bar{\mathbf{Z}}^a}{\partial \xi_2}}{\left| \dfrac{\partial \bar{\mathbf{Z}}^a}{\partial \xi_1} \times \dfrac{\partial \bar{\mathbf{Z}}^a}{\partial \xi_2} \right|} \tag{4}$$

Finite rotations about the three Cartesian axes, unlike infinitesimal rotations, do not qualify as vectors (Groesberg, /24/). The use of rotations of shell normal about the three global coordinate axes, which is a common practice in linear analysis of shells, has to be abandoned because the transformation and the updating of these rotations require special treatments when finite rotations are involved.

It has been noticed that in the rigid body dynamics, the rotational movement of a rigid body has been dealt with quite successfully by using Euler's angles (Gresberg, /24/), defined by a strict sequence of rotational displacements. The

transformation matrix can only represent two independent rotational modes, instead of three modes as required, thus indicating the shortcoming of Euler's angles when small rotation is specialized.

In Fig. 2, a new scheme proposed in this study is illustrated, which is based on another strict sequence of three successive rotations:

Transformation matrices for these rotations are :

$$R_1 = \begin{bmatrix} 1 & 0 & 0 \\ 0 & c_1 & -s_1 \\ 0 & s_1 & c_1 \end{bmatrix};\ R_2 = \begin{bmatrix} c_2 & 0 & s_2 \\ 0 & 1 & 0 \\ -s_2 & 0 & c_2 \end{bmatrix};\ R_3 = \begin{bmatrix} c_3 & -s_3 & 0 \\ s_3 & c_3 & 0 \\ 0 & 0 & 1 \end{bmatrix} \tag{5}$$

where $c_i = \cos\theta_i$, $s_i = \sin\theta_i$ $(i = 1,2,3)$ and the expression of transformation matrix **R** is

$$\mathbf{R} = R_1 R_2 R_3 = \begin{bmatrix} c_2\, c_3 & -c_2\, s_3 & s_2 \\ c_1\, s_3 + s_1\, s_2\, c_3 & c_1\, c_3 - s_1\, s_2\, s_3 & -s_1\, c_2 \\ s_1\, s_3 - c_1\, s_2\, c_3 & s_1\, c_3 + c_1\, s_2\, s_3 & c_1\, c_2 \end{bmatrix} \tag{6}$$

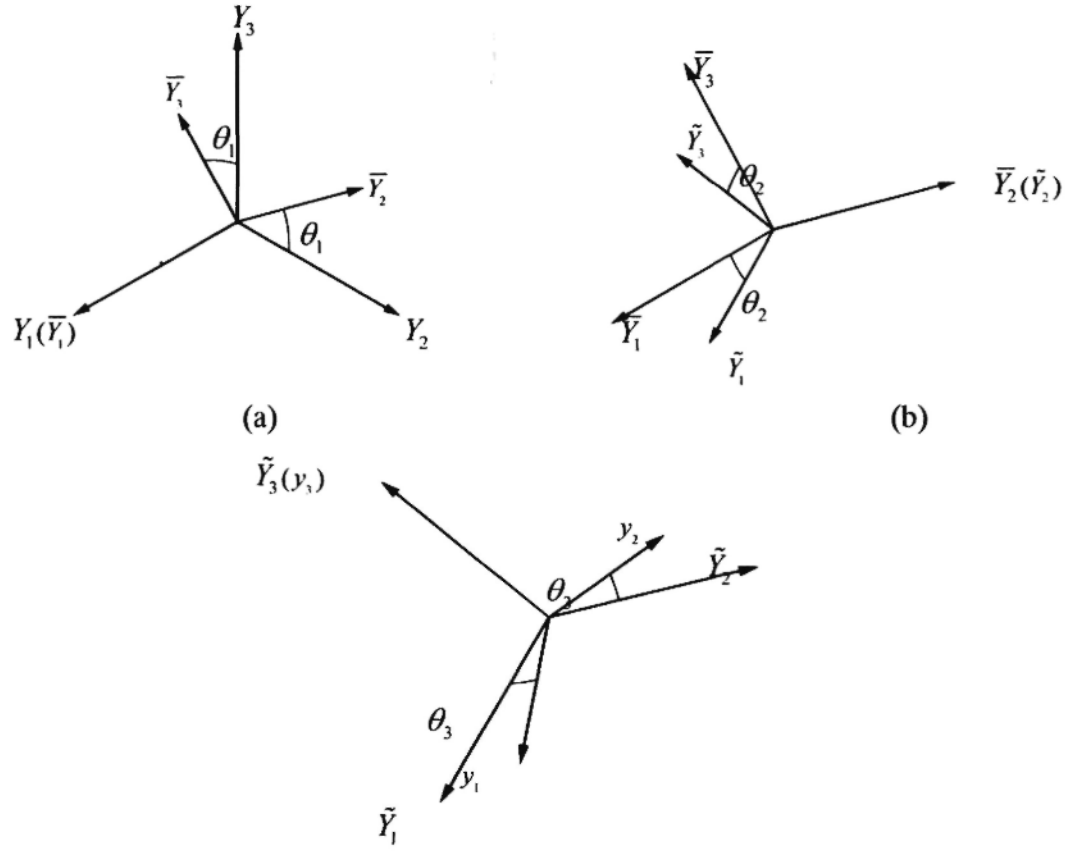

Fig. 2: Proposed rotation expression scheme, (a) A rotation, θ_1 , about Y_1 axis (b) A rotation, θ_2 , about $\bar{Y}_2$ axis, (c) A rotation, θ_3 , about $\tilde{Y}_3$ axis

The three rotations define a unique transformation matrix **R** through Equation (6); thus they can be used as generalized coordinate for the attached reference system at each node. Then the fiber displacement with respect to the mid-surface will be described by these three rotations.

The displacement field **u** in the shell element can be defined as

$$\mathbf{u}(\xi_i) = \sum_{a=1}^{9} N_a(\xi_\beta)\left[\bar{\mathbf{u}}^a + \xi_3 \frac{h^a}{2}\hat{\mathbf{e}}^a\right] = \bar{\mathbf{u}}(\xi_\beta) + \xi_3\,\bar{\mathbf{e}}(\xi_\beta) \tag{7}$$

where $\bar{\mathbf{u}}$ is the transitional displacement vector of a point in the mid-surface and $\hat{\mathbf{e}}^a$ is the fibre displacement vector at the node a, i.e.,

$$\hat{\mathbf{e}}^a = \mathbf{R}^a\hat{\mathbf{V}}^a - \hat{\mathbf{V}}^a \tag{8}$$

Consequently, using Eq. (8), the displacement field in Eq. (7) can be expressed as

$$\mathbf{u}(\xi_i) = \sum_{a=1}^{9} N_a(\xi_\beta)\left[\bar{\mathbf{u}}^a + \xi_3 \frac{h^a}{2}(\mathbf{R}^a - \mathbf{I}_{3\times 3})\hat{\mathbf{V}}^a\right] \tag{9}$$

where $\mathbf{I}_{3\times 3}$ is a unit matrix.

Assuming the three rotations of Eq. (6) are very small, one can obtain

$$\mathbf{u}(\xi_i) = \sum_{a=1}^{9} N_a(\xi_\beta)\left[\mathbf{I}_{3\times 3}\ \frac{\xi_3 h^a}{2}\Psi^a\right]\mathbf{u}^a(\xi_i) = \sum_{a=1}^{9}\mathbf{N}_a\mathbf{u}^a \tag{10}$$

where

$$\Psi^a = \begin{bmatrix} 0 & \hat{V}_3^a & -\hat{V}_2^a \\ -\hat{V}_3^a & 0 & \hat{V}_1^a \\ \hat{V}_2^a & -\hat{V}_1^a & 0 \end{bmatrix},\quad \mathbf{u}^a = \left\{\bar{u}_1^a, \bar{u}_2^a, \bar{u}_3^a, \theta_1^a, \theta_2^a, \theta_3^a\right\}^T,$$

$$\mathbf{N}_a = N_a\begin{bmatrix} 1 & 0 & 0 & 0 & 0 & 0 \\ 0 & 1 & 0 & 0 & 0 & 0 \\ 0 & 0 & 1 & 0 & 0 & 0 \\ 0 & 0 & 0 & 0 & \frac{\xi_3 h^a}{2}\hat{V}_3^a & -\frac{\xi_3 h^a}{2}\hat{V}_2^a \\ 0 & 0 & 0 & -\frac{\xi_3 h^a}{2}\hat{V}_3^a & 0 & \frac{\xi_3 h^a}{2}\hat{V}_1^a \\ 0 & 0 & 0 & \frac{\xi_3 h^a}{2}\hat{V}_2^a & -\frac{\xi_3 h^a}{2}\hat{V}_1^a & 0 \end{bmatrix}. \tag{11}$$

3. CONSTITUTIVE RELATIONS OF COMPOSITE LAMINATES

Since the present formulation is based on the natural co-ordinate reference frame, we introduce here an explicit transformation scheme between natural co-ordinates and the global co-ordinate system, to obtain a natural co-ordinate based constitutive equation. The stress tensor in the natural coordinate can be written as follows:

$$\bar{S}_{ij} = \bar{C}_{ijkl}\bar{E}_{kl} = \bar{J}_0 \mathbf{T}\bar{D}_{ijkl}\mathbf{T}^{\mathbf{T}}\bar{E}_{kl} \tag{12}$$

where $\bar{J}_0$ is the determinant of the Jacobian matrix, $\bar{D}_{ijkl}$ is the constitutive matrix for orthotropic materials with the material angle θ. The transformation matrix $\mathbf{T}$ in Eq. (12) is given as

$$\mathbf{T} = \begin{bmatrix} \chi_{1111} & \chi_{2121} & \chi_{3131} & 2\chi_{1121} & 2\chi_{2131} & 2\chi_{1131} \\ \chi_{1212} & \chi_{2222} & \chi_{3232} & 2\chi_{1222} & 2\chi_{2232} & 2\chi_{1232} \\ \chi_{1313} & \chi_{2323} & \chi_{3333} & 2\chi_{1323} & 2\chi_{2333} & 2\chi_{1333} \\ \chi_{1112} & \chi_{2122} & \chi_{3132} & \chi_{1122}+\chi_{1221} & \chi_{2132}+\chi_{2231} & \chi_{1132}+\chi_{1231} \\ \chi_{1213} & \chi_{2223} & \chi_{3233} & \chi_{1223}+\chi_{1322} & \chi_{2233}+\chi_{2332} & \chi_{1233}+\chi_{1332} \\ \chi_{1113} & \chi_{2123} & \chi_{3133} & \chi_{1123}+\chi_{1321} & \chi_{2133}+\chi_{2331} & \chi_{1133}+\chi_{1331} \end{bmatrix} \tag{13}$$

where

$$\chi_{ijkl} = \frac{\partial \xi_j}{\partial \mathbf{Z}_i}\frac{\partial \xi_l}{\partial \mathbf{Z}_k} \tag{14}$$

Substituting Eq. (12) into the strain energy equation of the shell represented as a three-dimensional body can be expressed by

$$U = \frac{1}{2}\int_A \int_{-h/2}^{h/2} \bar{E}_{ij}^T \bar{C}_{ijkl}\bar{E}_{kl}\, d\xi_3\, dA \tag{15}$$

After integration throughout the thickness, the strain energy can be obtained in terms of shell quantities: stress resultants and couples and laminated shell stiffness characteristics

$$A_{\alpha\beta\gamma\delta}, B_{\alpha\beta\gamma\delta}, D_{\alpha\beta\gamma\delta} = \int_{-h/2}^{h/2} \bar{C}_{\alpha\beta\gamma\delta}\,(1, \xi_3, \xi_3^2)\, d\xi_3,$$
$$A_{\alpha 3\beta 3} = k_s \int_{-h/2}^{h/2} \bar{C}_{\alpha 3\beta 3}\, d\xi_3 \tag{16}$$

The value of 5/6 (Whitney /25/) is used as the transverse shear correction factor (k_s) in the finite element formulation.

The shell element displays resultant forces acting on a laminate which are obtained by integration of stresses through the laminate thickness. In this study, we impose the plane state on the natural constitutive equation of Eq. (12) before forming the equivalent constitutive equation. The constitutive relations of the composite laminate are as follows:

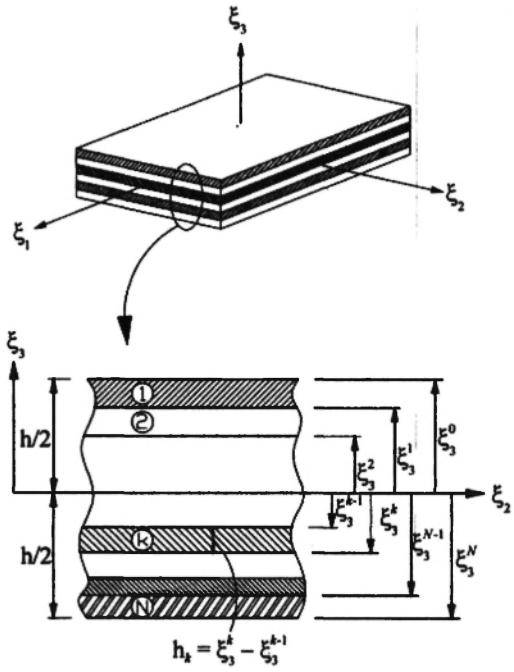

Fig. 3: Cross-section of laminated plate composed of N layers.

$$\begin{Bmatrix} N_{\alpha\beta} \\ M_{\alpha\beta} \\ Q_{\alpha 3} \end{Bmatrix} = \begin{bmatrix} A_{\alpha\beta\gamma\delta} & B_{\alpha\beta\gamma\delta} & 0 \\ B_{\alpha\beta\gamma\delta} & D_{\alpha\beta\gamma\delta} & 0 \\ 0 & 0 & A_{\alpha 3\beta 3} \end{bmatrix} \begin{Bmatrix} \bar{E}^m_{\gamma\delta} \\ \bar{E}^b_{\gamma\delta} \\ \bar{E}^s_{\beta 3} \end{Bmatrix} \tag{17}$$

4. TORSIONAL STIFFNESS FOR COMPOSITE STIFFENED PLATE

To model composite stiffened plates, the need for six degrees of freedom arises because the process of stiffness accumulation at any node lying on the junction must be carried out in a single reference frame. However, it is well known that this creates problems associated with rotation about the normal to the shell mid-surface. Initially, this torsional degree of freedom was specified in global co-ordinates but this leads to singularity problems when adjacent elements are exactly co-planar. This difficulty is overcome by providing a fictitious torsional spring along the local normal direction at each node of the element. However, this technique has the drawback that it interferes with the ability of the element to undergo strain free rigid body motions. Kanok-Nukulchai /26/ used an additional constraint to link the torsional rotation to the average in-plane rotation of the mid-surface. Adopting the continuum mechanics definition, the constraint equation can be written as follows:

$$\alpha_t(\xi_1,\xi_2) - \frac{1}{2}\left\{\frac{\partial w_2}{\partial z_1}(\xi_1,\xi_2,0) - \frac{\partial w_1}{\partial z_2}(\xi_1,\xi_2,0)\right\} \approx 0 \tag{18}$$

where α_t is the in-plane torsional rotation; w_1 and w_2 are displacement components in the local coordinate system for expression of torsional energy; $z_i\ (i = 1,2,3)$ are local Cartesian coordinates with z_3 axis normal to the shell mid-surface.

In this study, based on the procedure proposed by Kanok-Nukulchai /26/, the drilling degree of freedom will be tied to the in-plane twist by a penalty functional through an additional strain energy as

$$U_t = k_t G \int_{V^e} \left[\alpha_t(\xi_1,\xi_2) - \frac{1}{2}\left\{ \frac{\partial w_2}{\partial z_1}(\xi_1,\xi_2,0) - \frac{\partial w_1}{\partial z_2}(\xi_1,\xi_2,0) \right\} \right]^2 dV \tag{19}$$

where k_t is a parameter to be determined (the value of 0.1 suggested); G is the shear modulus; V^e is the volume of the element; and dV is the volume element. A two-by-two Gauss integration scheme is applied for the evaluation of the torsional stiffness in order to avoid the over-constrained situation. After integration throughout the thickness, Eq. (19) can be written as

$$U_t = 2k_t G \int_{-1}^{1}\int_{-1}^{1} \left[\alpha_t(\xi_1,\xi_2) - \frac{1}{2}\left\{ \frac{\partial w_2}{\partial z_1}(\xi_1,\xi_2,0) - \frac{\partial w_1}{\partial z_2}(\xi_1,\xi_2,0) \right\} \right]^2 d\xi_1\, d\xi_2 \tag{20}$$

To derive a torsional stiffness from Eq. (20) the local variables are expressed in terms of global nodal variables by shape functions and using virtual work principle. This gives Eq. (20) in the form

$$\delta U_t = \delta \mathbf{u}^T \mathbf{K}_{\mathbf{tL}} \mathbf{u} \tag{21}$$

Since the virtual displacement $\delta \mathbf{u}$ is arbitrary, the torsional stiffness matrix ($\mathbf{K}_{\mathbf{tL}}$) can obtain. A two-by-two Gauss integration scheme is applied for the evaluation of the torsional stiffness in order to avoid the over-constrained situation and the torsional stiffness term was added as described in Kanok-Nukulchai /26/.

5. NATURAL STRAIN TENSOR AND STRAIN INTERPOLATION

Following the natural co-ordinate system (Han *et al.*, /18/), the natural strain tensor corresponding to the Green strain tensor may be defined as

$$\bar{E}_{\alpha\beta} = \frac{\partial \mathbf{Z}_I}{\partial \xi_\alpha}\frac{\partial \mathbf{Z}_J}{\partial \xi_\beta} E_{IJ} \tag{22}$$

It should be noted that the Green strain tensor and the natural strain have the following tensor transformation relationship.

$$\bar{E}_{\alpha\beta} - \frac{1}{2}\left[\frac{\partial \mathbf{Z}_I}{\partial \xi_\alpha}\frac{\partial \mathbf{u}_I}{\partial \xi_\beta} + \frac{\partial \mathbf{u}_J}{\partial \xi_\alpha}\frac{\partial \mathbf{Z}_J}{\partial \xi_\beta} \right] \tag{23}$$

The strain expressions in Eq. (23) can be expressed as :

$$\bar{E}^m = \bar{\mathbf{B}}_\mathbf{m}\, \bar{\mathbf{u}}\ ,\ \bar{E}^b = \xi_3 \bar{\mathbf{B}}_\mathbf{b}\, \mathbf{u}\ ,\ \bar{E}^s = \bar{\mathbf{B}}_\mathbf{s}\, \mathbf{u}\ . \tag{24}$$

where $\bar{E}^m$, $\bar{E}^b$ and $\bar{E}^s$ are membrane, bending and transverse shear strain components. and the strain-displacement

matrices $\bar{\mathbf{B}}_m$, $\bar{\bar{\mathbf{B}}}_b$ and $\bar{\mathbf{B}}_s$ are presented in Han *et al.* /18/.

In order to avoid locking problems, the assumed natural strain method in the 9-node shell element by Han *et al.* /18/ is used. Thus the transverse shear and membrane strain fields are interpolated with the following sampling points in Fig. 4.

$$\bar{e}_{13}=\sum_{i=1}^{2}\sum_{j=1}^{3}\Omega_i(\xi_1)\Xi_j(\xi_2)\bar{E}_{13}^{\lambda},\ \bar{e}_{23}=\sum_{i=1}^{2}\sum_{j=1}^{3}\Omega_i(\xi_2)\Xi_j(\xi_1)\bar{E}_{23}^{\lambda},\ \bar{e}_{12}=\sum_{i=1}^{2}\sum_{j=1}^{2}\Omega_i(\xi_1)\Omega_j(\xi_2)\bar{E}_{12}^{\lambda}. \tag{25}$$

where $\lambda=2(j-1)+i$ denotes the position of the sampling point as shown in Fig. 4 and the shape functions $\Omega_i(\xi_1)$ and $\Xi_j(\xi_2)$ are

$$\Omega_1(\xi_1)=\frac{1}{2}\left(1+\sqrt{3}\xi_1\right),\ \Omega_2(\xi_1)=\frac{1}{2}\left(1-\sqrt{3}\xi_1\right),$$
$$\Xi_1(\xi_2)=\frac{1}{2}\xi_2(\xi_2+1),\ \Xi_2(\xi_2)=1-\xi_2^2,\ \Xi_3(\xi_2)=\frac{1}{2}\xi_2(\xi_2-1). \tag{26}$$

in which $\Omega_i(\xi_2)$ and $\Xi_i(\xi_1)$ can be obtained by changing variables. The assumed strain $\bar{e}_{11}$, $\bar{e}_{22}$ have the same interpolation scheme as $\bar{e}_{13}$, $\bar{e}_{23}$, respectively.

The assumed strains $\bar{\mathbf{e}}$ derived from Eq. (25) are used in the present shell element instead of the strains $\bar{E}$ of Eq. (24) obtained from the displacement field. In this study, a $\bar{\mathbf{B}}_{\mathbf{AS}}$ matrix is implemented from assumed natural strains instead of using the standard $\bar{\mathbf{B}}$ matrix as shown in Eq. (26).

$$\begin{Bmatrix}\bar{\mathbf{e}}^m\\ \bar{E}^b\\ \bar{\mathbf{e}}^s\end{Bmatrix}=\begin{bmatrix}\left(\bar{\mathbf{B}}_{\mathbf{m}}\right)_{\mathbf{AS}} & 0\\ \xi_3\bar{\mathbf{B}}_{\mathbf{b1}} & \xi_3\bar{\mathbf{B}}_{\mathbf{b2}}\\ \left(\bar{\mathbf{B}}_{\mathbf{s1}}\right)_{\mathbf{AS}} & \left(\bar{\mathbf{B}}_{\mathbf{s2}}\right)_{\mathbf{AS}}\end{bmatrix}\begin{Bmatrix}\bar{\mathbf{u}}\\ \boldsymbol{\theta}\end{Bmatrix} \tag{27}$$

where $\bar{\mathbf{e}}^m$ and $\bar{\mathbf{e}}^s$ are assumed membrane and assumed transverse shear strain components.

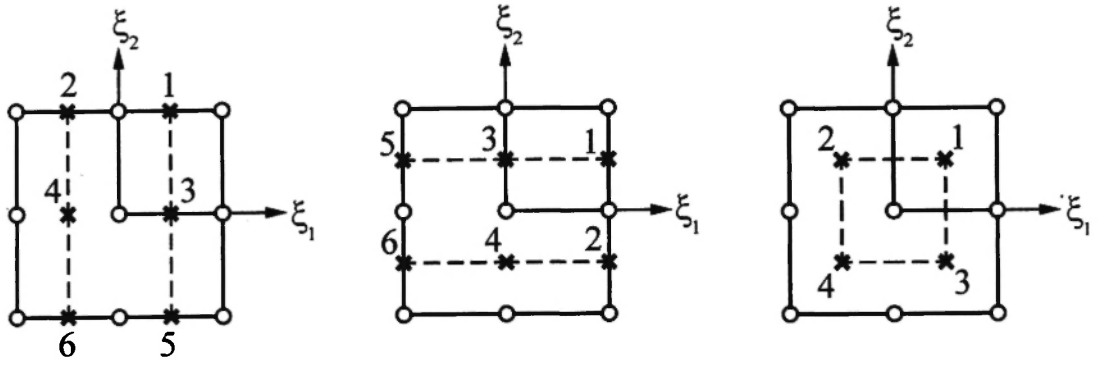

Fig. 4: Sampling points for assumed strains of $\bar{e}_{11}$, $\bar{e}_{13}$, $\bar{e}_{22}$, $\bar{e}_{23}$ and $\bar{e}_{12}$

6. DYNAMIC EQUILIBRIUM EQUATION

Using virtual work principle, the following dynamic equilibrium equation is obtained based on the membrane, bending and transverse shear resultant forces.

$$\int\left(\delta\left(\bar{e}^{m}_{\gamma\delta}\right)^{T} N_{\alpha\beta}+\delta\left(\bar{E}^{b}_{\gamma\delta}\right)^{T} M_{\alpha\beta}+\delta\left(\bar{e}^{s}_{\beta 3}\right)^{T} Q_{\alpha 3}\right)dA = \int\rho\,\delta\mathbf{u}^{T}\ddot{\mathbf{u}}\,dV \tag{28}$$

where ρ is the density of the element material.

Since the virtual displacement $\delta\mathbf{u}$ is arbitrary, the Eq. (28) may be written as

$$\mathbf{K_L u} - \mathbf{M}\,\ddot{\mathbf{u}} = 0 \tag{29}$$

where

$$\mathbf{K_L} = \int\begin{bmatrix}\mathbf{K_L^{11}} & \mathbf{K_L^{12}}\\ \mathbf{K_L^{21}} & \mathbf{K_L^{22}}\end{bmatrix}dA \tag{30}$$

in which the sub-matrix of $\mathbf{K_L}$ is shown in Han *et al.* /18/,

and

$$\mathbf{M} = \int\rho\begin{bmatrix}\left(\mathbf{N}_a^{T}\mathbf{N}_b\right)^{11}_{3\times 3} & 0\\ 0 & \left(\mathbf{N}_a^{T}\mathbf{N}_b\right)^{22}_{3\times 3}\end{bmatrix}_{6\times 6} dV \tag{31}$$

where

$$\left(\mathbf{N}_a^{T}\mathbf{N}_b\right)^{11} = \begin{bmatrix}N_aN_b & 0 & 0\\ 0 & N_aN_b & 0\\ 0 & 0 & N_aN_b\end{bmatrix},$$

$$\left(\mathbf{N}_a^{T}\mathbf{N}_b\right)^{22} = N_aN_b\begin{bmatrix}\xi_3^2\frac{h^ah^b}{4}\left(\hat{V}_3^a\hat{V}_3^b+\hat{V}_2^a\hat{V}_2^b\right) & -\xi_3^2\frac{h^ah^b}{4}\hat{V}_2^a\hat{V}_1^b & -\xi_3^2\frac{h^ah^b}{4}\hat{V}_3^a\hat{V}_1^b\\ -\xi_3^2\frac{h^ah^b}{4}\hat{V}_1^a\hat{V}_2^b & \xi_3^2\frac{h^ah^b}{4}\left(\hat{V}_3^a\hat{V}_3^b+\hat{V}_1^a\hat{V}_1^b\right) & -\xi_3^2\frac{h^ah^b}{4}\hat{V}_3^a\hat{V}_2^b\\ -\xi_3^2\frac{h^ah^b}{4}\hat{V}_1^a\hat{V}_3^b & -\xi_3^2\frac{h^ah^b}{4}\hat{V}_2^a\hat{V}_3^b & \xi_3^2\frac{h^ah^b}{4}\left(\hat{V}_2^a\hat{V}_2^b+\hat{V}_1^a\hat{V}_1^b\right)\end{bmatrix} \tag{32}$$

in which N_a and N_b are the shape function at node a and b. The Lanczos method which was used in Park *et al.* /6/, is employed to solve Eq. (29).

7. NUMERICAL EXAMPLES

7.1 Vibration of laminated composite plates

The examples of square anti-symmetric cross-ply and angle-ply laminated composite plates with various layer stacking sequence are shown in Fig. 5. In this study, all the plates are analyzed with 10 × 10 mesh. The fibers of the top and bottom layers are in the direction of x-axis. These examples are examined using both Navier's method with first-order shear deformation theory (Reddy, /2/) and finite element method with lumped mass (Han and Choi /5/). The material properties and geometry are as follow:

$E_1 = 40$, $E_2 = 1$, $G_{12} = G_{13} = 0.6$, $G_{23} = 0.5$, $\nu_{12} = 0.25$, $\rho = 1$.

The plate is simply supported and can be analyzed by means of the following boundary conditions:

$x = 0, a : \bar{u}_2 = \bar{u}_3 = \theta_1 = 0$, $y = 0, b : \bar{u}_1 = \bar{u}_3 = \theta_2 = 0$.

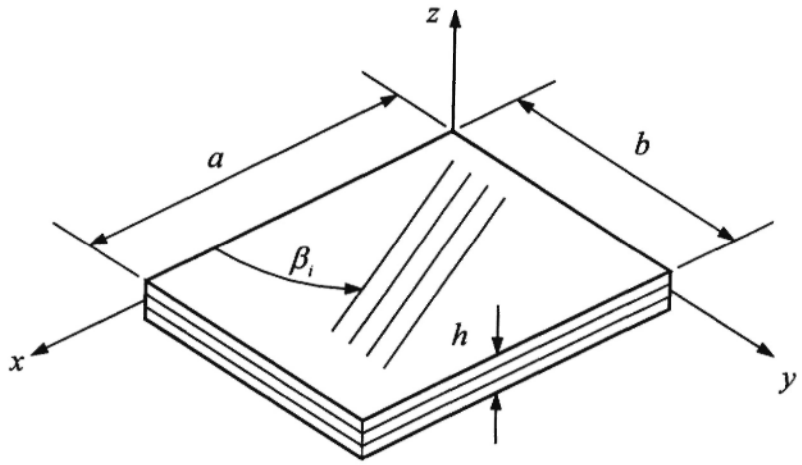

Fig. 5: Geometry of laminated plates

In Table 1, the results of the present study are compared with both Navier solution with first-order shear deformation theory (FSDT) and the finite element solution by Han and Choi /5/. The present test results show very good agreement with the references.

7. 2 Vibration of the isotropic stiffened plate

The vibration of clamped isotropic plate with a single stiffener is examined. For the present single ribbed square plate, the experimental natural frequencies were measured in Olsen and Hazell /8/. The geometry and material properties are as follow:

$a = b = 203\,mm$, $h = 1.37\,mm$, $t_s = 6.35\,mm$, $h_s = 12.7\,mm$, $E = 68.7\,\text{GPa}$, $\nu = 0.3$, $\rho = 2820\,kg/m^3$.

Table 1

Non-dimensional first frequency ($\bar{\varpi} = \varpi\sqrt{\rho h^2 / E_2}$, a/b=1, a/h=10) of the laminated composite plates

Solutions	Anti-symmetric Cross-ply [a]		Anti-symmetric Angle-ply			
	n=2	n=10	n=2 [b]	n=4 [c]		n=10 [d]
FSDT (Reddy, /2/)	10.473	15.779	13.044	14.742	17.634	19.380
Han and Choi /5/	10.534	15.823	13.100	-	-	19.391
Present	10.477	15.779	13.044	14.742	17.634	19.381

[a] 0/90, $(0/90)_5$; [b] 45/-45 ; [c] $(5/-5)_2$, $(30/-30)_2$; [d] $(45/-45)_5$

The present results were obtained using the mesh 10 × 10 for the plate and 1 × 10 for the stiffener. A consistent mass matrix was employed in Eq. (28). The Olson and Hasell /8/, Rikards *et al.* /13/ and present results are presented in Table 2, where it is shown that the best agreement with the experiment and ANSYS is for numerical frequencies computed by present shell element. For comparison numerical frequencies have also been calculated employing the code ANSYS. In this case, the mesh 24 × 24 was used and the assembly of the shell elements for the skin and stiffener was employed.

Generally, all frequencies of present analysis employing the shell model with assumed natural strain formulation for the plate and stiffener are closer to the experiment and ANSYS than other references.

7. 3 Vibration of the composite stiffened plate with angle-ply single rib

In order to verify the present assumed natural strain shell model for a composite stiffener, we compared the results of the present shell model with those of a beam model for stiffened anisotropic plate. In general, the symmetric vibration mode in the isotropic plates does not always become a symmetric mode in the anisotropic plates. Thus the full finite element modeling should be used for stiffened anisotropic plates. Numerical results are obtained for the composite stiffened plate made of a carbon-epoxy composite materials (AS1/3501-6). The properties of that material are listed in Table 3.

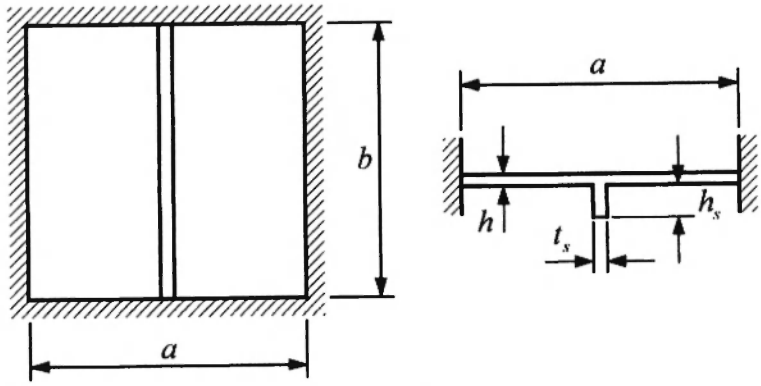

Fig. 6: Stiffened isotropic plate with all clamped boundary conditions

Table 2
Natural frequencies [Hz] of isotropic stiffened plate

Mode	Olson & Hazell /8/		Lee *et al.* /12/	Rikards *et al.* /13/	ANSYS (Rikards *et al.*, /13/)	Present
	Theory	Experiment				
1	718.1	689	711.1	693.2	712.6	720.7
2	751.4	725	743.4	751.0	742.9	747.2
3	997.4	961	975.2	984.8	983.8	989.6
4	1007.1	986	993.4	1007	993.6	999.1
5	1419.8	1376	1414.5	1417	1398.5	1408.1
6	1424.3	1413	1423.0	1427	1402.5	1411.5
7	1631.5	1512	1552.9	1651	1599.5	1612.9
8	1853.9	1770	1886.6	1829	1831.0	1866.8
9	2022.8	1995	2024.6	2019	1983.6	2003.9
10	2025.0	2069	2064.1	2024	1985.8	2005.8
11	2224.9	2158	-	2191	2175.6	2209.4
12	2234.9	2200	-	2231	2185.0	2214.4
13	2400.9	2347	-	2393	2344.6	2380.3
14	2653.9	2597	-	2645	2585.9	2619.7
15	2670.2	2614	-	2674	2597.5	2629.9
16	2802.4	2784	-	2789	2733.9	2783.2
17	2804.6	2784	-	2793	2735.1	2784.3
18	3259.0	3174	-	3254	3143.7	3185.0
19	3265.9	3174	-	3271	3148.8	3189.4
20	3414.2	3332	-	3583	3316.8	3434.2
21	3754.0	3660	-	3724	3644.3	3760.7
22	3754.8	3730	-	3726	3644.8	3761.1
23	3985.5	3780	-	3909	3798.8	3916.3
24	4045.9	3913	-	4019	3862.9	3929.1

Table 3
Material properties of the composite stiffened plate

Material	E_1	E_2	$G_{12} - G_{13}$	G_{23}	ν_{12}	ρ	Ply thickness
Carbon-epoxy (AS1/3501-6)	128 [GPa]	11 [GPa]	4.48 [GPa]	1.53 [GPa]	0.25	1500 [kg / m^3]	0.13 [mm]

The lamination scheme of the skin plate is $(0/\pm 45/90)_s$ and the $(0_3/\pm\theta_3)_s$ composite stiffener is used to investigate the effect of the fiber orientation of the stiffener on the natural frequency. The boundary conditions and geometry are presented Fig. 7. The size of the stiffener is $t_s = 2.34\,mm$ and $h_s = 30.0\,mm$. The mesh of the skin plate is 10×10. The results are presented in Fig. 8. Lee *et al.* /12/ showed that the frequencies of first and third modes were dependent on the fiber orientation of the stiffener and the stiffener with 30 ply angle had the maximum values of the frequencies. But there is almost no change in the frequencies. It can also be observed from Fig. 8 that the stiffener should be idealized by using the shell elements.

In Fig. 9, the lamination scheme of the skin plate is $(0/\pm\theta/90)_s$ and the $(0_3/\pm 45_3)_s$ composite stiffener is used to study the effect of the fiber orientation of the skin plate on the natural frequency. As shown in Fig. 9, the skin plate with 35 – 40 ply angle has the maximum values of the first natural frequency. The first frequencies of two types of lamination scheme are presented in Fig. 10. The fiber orientation of the skin plate is more significant than the fiber orientation of the stiffener.

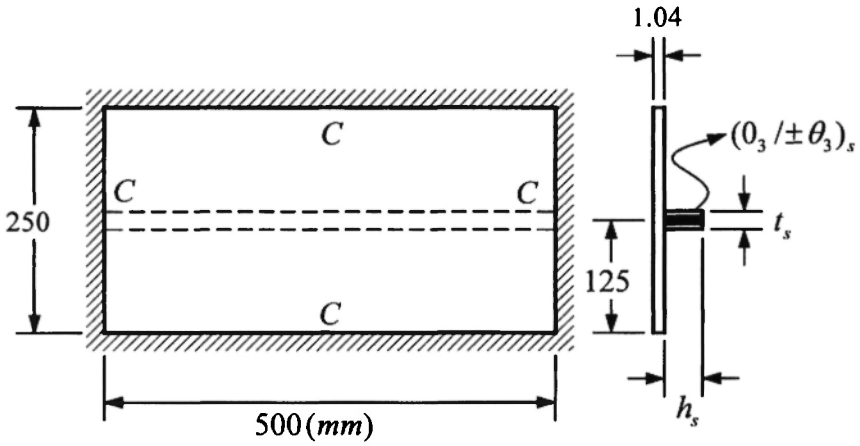

Fig. 7: Laminated composite plate with stiffener

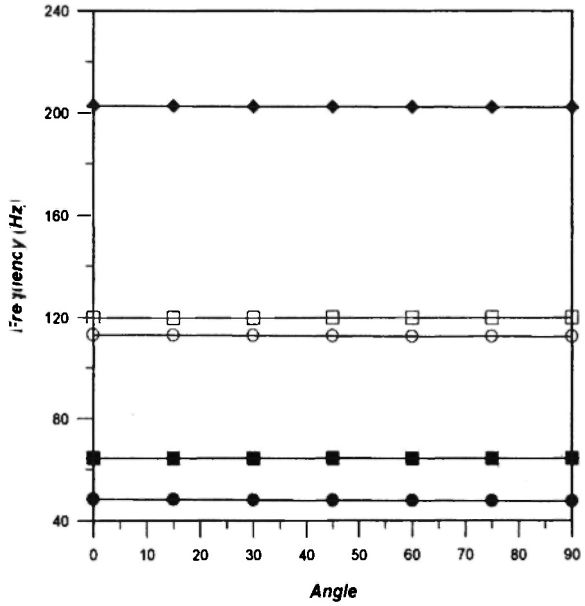

Fig. 8: Effect of the fiber orientation of stiffener on natural frequencies

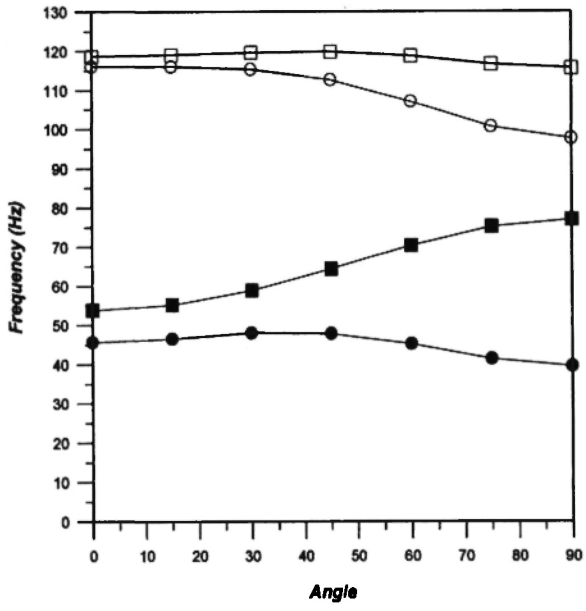

Fig. 9: Effect of the fiber orientation of skin plate on natural frequencies

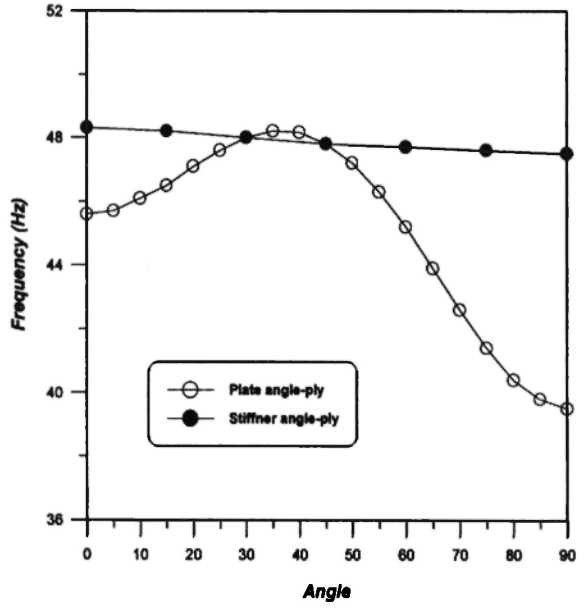

Fig. 10: Effect of the fiber orientation of skin plate and stiffener on first natural frequencies

7. 4 Vibration of the composite stiffened plate with double stiffener

The dimensions of the doubly stiffened laminated composite plate are presented in Fig. 11. The layer-up of the skin plate and stiffener are $(0_2/\pm 45_2/90_2)_s$ and $(0_4/90_4)_s$, respectively. Results are compared with the Lee *et al.* /12/ in Table 4. Table 4 shows the effect of the location of stiffeners on the frequencies. As the location of stiffeners becomes farther from the center line, the frequency of the lowest five modes goes up and down. The frequencies are severely

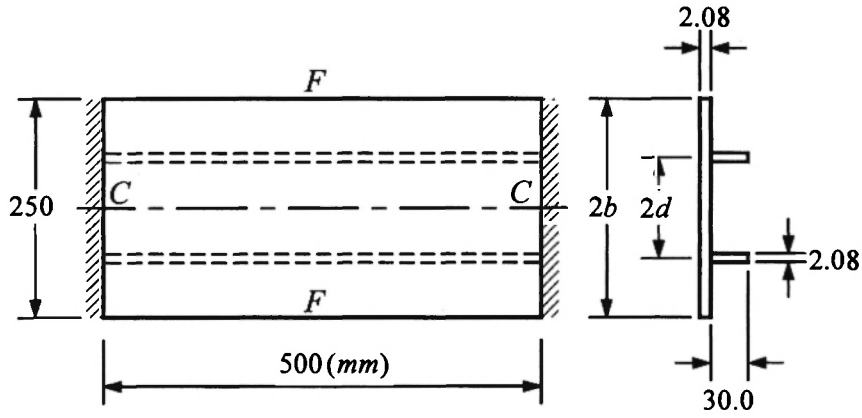

Fig. 11: Anisotropic plate with double stiffeners

Table 4
Natural frequencies of doubly stiffened plates

Stiffener location (d/b)	Frequencies of five modes [Hz]									
	1		2		3		4		5	
	a	b	a	b	a	b	a	b	a	b
0.2	138.2	138.5	141.2	139.3	252.3	256.3	259.2	262.2	424.1	431.8
0.4	170.3	171.3	200.7	194.6	294.8	299.8	318.1	319.3	471.4	425.6
0.6	189.8	192.5	301.7	300.2	326.4	330.9	382.3	357.2	434.6	444.2
0.8	144.2	145.9	266.2	271.9	375.2	372.6	438.5	451.0	499.0	504.6
1.0	110.7	111.7	227.9	232.4	269.1	268.4	372.7	385.4	409.2	413.5

a : Lee *et al.* /12/, b : Present

dependent on the location of the stiffeners. As shown in Table 4 the proper location to increase the fundamental frequency is a position about 60% from the center line. The present and reference fundamental frequency of position (d/b=0.6) showed the difference of about 1.4%. The first three mode shapes of five models are shown in Fig. 12. The ansymmetric first mode about the stiffener becomes the symmetric mode as the distance of stiffener increases.

7. 5 Vibration of the composite stiffened plate under in-plane load

The stacking sequence of the skin plate is $(0/90/90/0)$ and the $(45/-45/-45/45)$ composite stiffener is used to investigate the effect of the combination of in-plane compression and shear loading on the natural frequency. The dimensions of stiffened plate are presented in Fig. 7. The geometry and material properties are as follow:

Stiffener location (d/b)	First mode	Second mode	Third mode
0.2	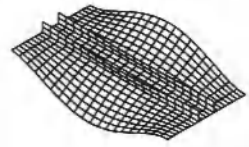	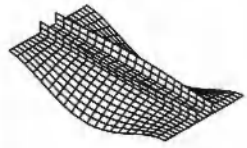	
0.4	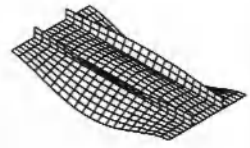	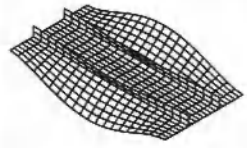	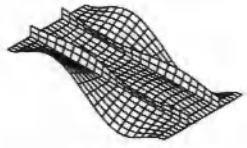
0.6	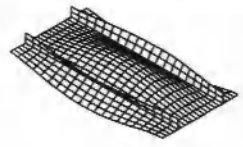		
0.8	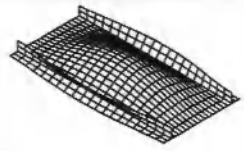	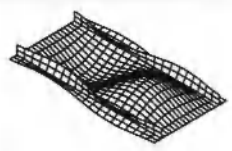	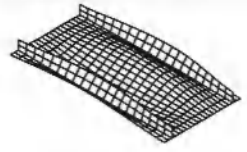
1.0	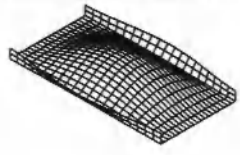		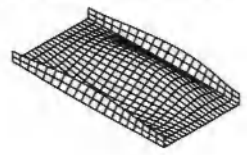

Fig. 12: Mode shapes of doubly stiffened plates

$a = b = 10.0\,m$, $h = 1.0\,m$, $t_s = 1.0\,m$, $h_s = 2.0\,m$, $\rho = 1.0\times10^{10}\ N\cdot\sec^2/m^4$, $E_1 = 40\,E_2$, $E_2 = 1.0\times10^{10}\ N/m^2$, $G_{12} = G_{13} = 0.6\,E_2$, $G_{23} = 0.5\,E_2$, $\nu = 0.25$.

The boundary conditions are as follow:

$x = 0, 10\,m$: $u_3 = \theta_1 = \hat{\sigma}_3 = 0$, $y = 0, 10\,m$: $u_3 = \theta_2 = \hat{\sigma}_3 = 0$, $z = 0, -2\,m$: $u_1 = \theta_1 = 0$.
(for stiffener)

The mesh of the skin plate is 10 × 10. The types of in-plane compression and shear loading are presented in Fig. 13. The results are presented in the non-dimensional form using the equation:

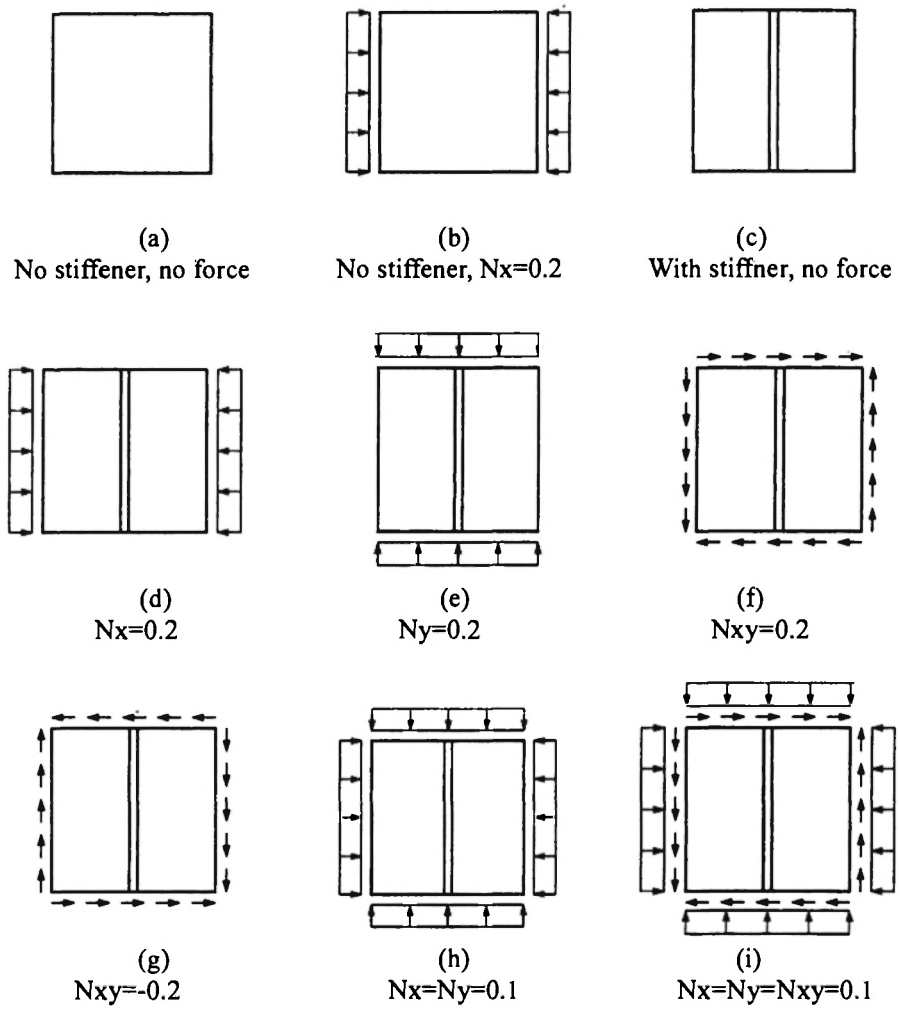

Fig. 13: Load types for stiffened plate with in-plane loads

$$\bar{f} = f\left(\frac{a^2}{h}\sqrt{\frac{\rho}{E_2}}\right) \tag{33}$$

The results are presented in Table 5 and Fig. 14. In case (b), the in-plane compressive load reduces the natural frequencies of un-stiffened plate about 62.1%. Therefore, we can predict the buckling load using the vibration analysis. But in-plane shear load increases the natural frequencies. The combination of in-plane compression and shear loading has influence on the change of the natural frequency according to the magnitude of the in-plane compression and shear load, respectively. In case (i), the variation of the frequencies are very small. Thus, the magnitude, direction of the in-plane compression and shear loading in laminated composite stiffened plates should be selected properly to control the specific frequency and mode shape.

Fig. 15 illustrates the dynamic behaviour of the composite stiffened plate. The aim of this example is to investigate the resonant frequency characteristic under in-plane compression loading. The intersection, between the curves, interchanges the sequence of some of the mode shapes as a result of the increase in the in-plane compressive load. It is

Table 5
Natural frequencies of composite stiffened plates under in-plane load

Type	Frequencies [$\bar{f}$]				
	First mode	Second mode	Third mode	Fourth mode	Fifth mode
(a)	2.410	5.124	6.136	7.427	7.667
(b)	0.913	4.211	4.608	6.234	6.683
(c)	2.266	4.172	4.933	5.650	6.150
(d)	1.256	4.172	4.230	4.566	5.651
(e)	1.262	3.049	4.153	4.525	5.599
(f)	3.832	3.955	4.166	5.235	5.455
(g)	3.825	3.954	4.166	5.235	5.451
(h)	1.474	3.992	4.159	5.334	5.624
(i)	2.157	3.216	3.713	3.931	4.159

related to the change in the number of half-waves which are parallel to the load direction. The various mode shapes have been defined in Fig. 16. These values are known to be the points at which the intersections between the different sets of curves, shown in Fig. 15, occur.

Figs. 17-20 illustrate the dynamic behaviors of the composite stiffened plates subjected to the combination of in-plane shear and unidirectional compressive loads. The effect of the applied shear and in-plane compressive loads is shown. As expected, the natural frequencies of composite stiffened plates with shear loads exhibit higher values than the case of without shear loads as shown in Fig. 17 and Fig. 19.

Fig. 21 shows the natural frequencies of the composite stiffened plates under the combination of in-plane shear and bidirectional compressive loads. As expected, the natural frequencies of composite stiffened plates are decreased when the in-plane bidirectional compressive loads increase. However, the buckling load of composite stiffened plate decreases when compared with the case of the in-plane unidirectional compressive loads. Similar to the case of only in-plane compressive load, the intersection, between the curves, interchanges the sequence of some of the mode shapes as a result of the increase in the in-plane compressive loads in Fig. 17, Fig. 19 and Fig. 21.

7. 6 Vibration of the composite stiffened plate with angle-ply skin plate under in-plane shear and compression

Fig. 22 illustrates the dynamic behaviour of the composite stiffened plate with symmetric and antisymmetric angle-ply skin plate. The stacking sequence of the skin plate is $(\theta/-\theta/-\theta/\theta)$, $(\theta/-\theta/\theta/-\theta)$ and the $(45/-45/-45/45)$

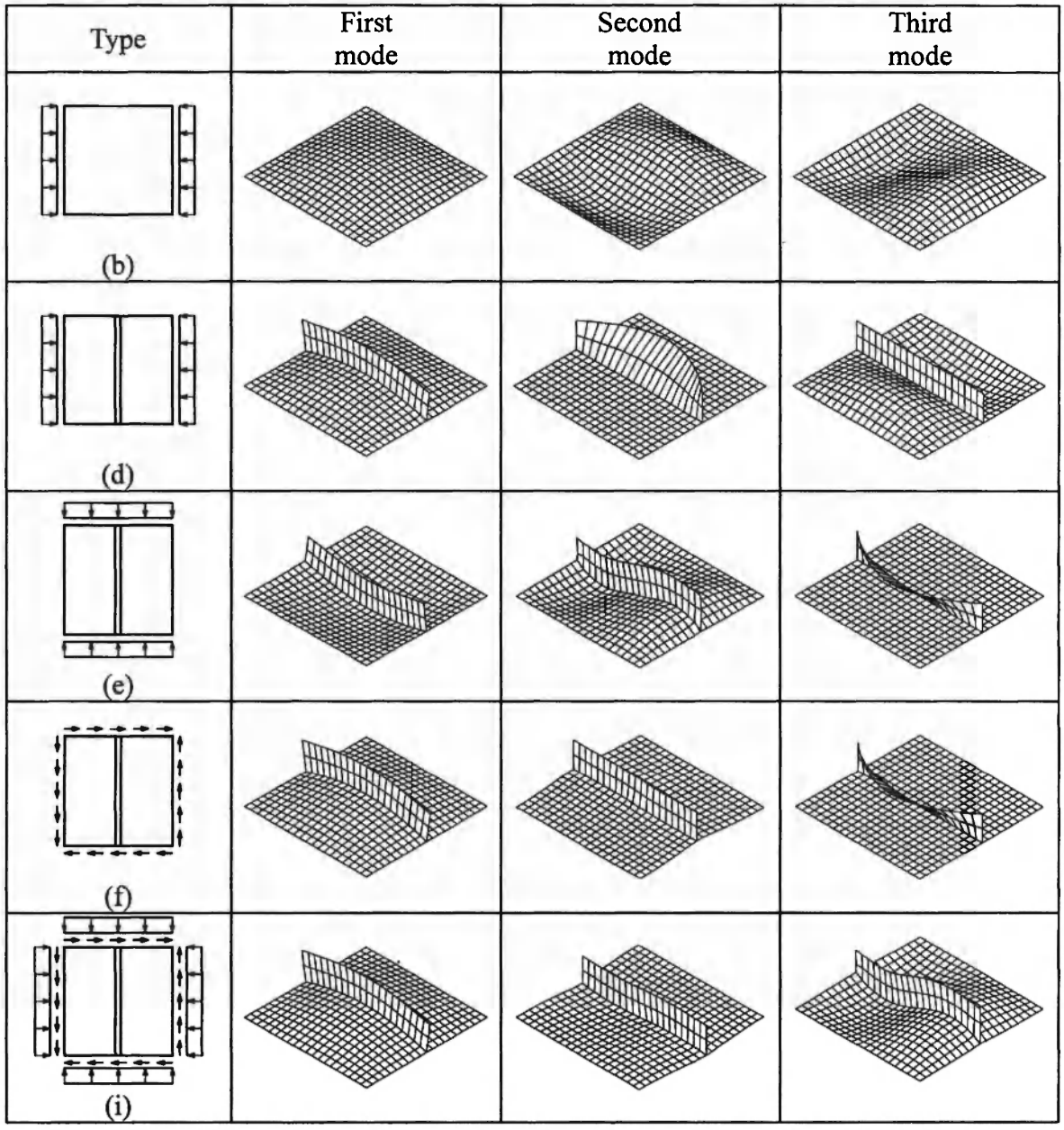

Fig. 14: Mode shapes of stiffened plates under in-plane loadings

composite stiffener is used to investigate the effect of the variation of fiber angle on the natural frequency. The intersection, between the curves, interchanges the sequence of some of the mode shapes as a result of the increase in the fiber angle. It is related to the change in the number of half-waves which are parallel to the load direction. Fig. 23 shows that the antisymmetric laminated composite plates have larger fundamental frequency and intersection point than the symmetric plates.

Fig. 24 illustrates the dynamic behaviour of the composite stiffened plate with antisymmetric angle-ply skin plate. The stacking sequence of the skin plate is $(\theta/-\theta)$, $(\theta/-\theta)_2$, $(\theta/-\theta)_4$ and the $(45/-45/-45/45)$ composite stiffener is used to investigate the effect of the variation of fiber angle and number of layers on the natural frequency.

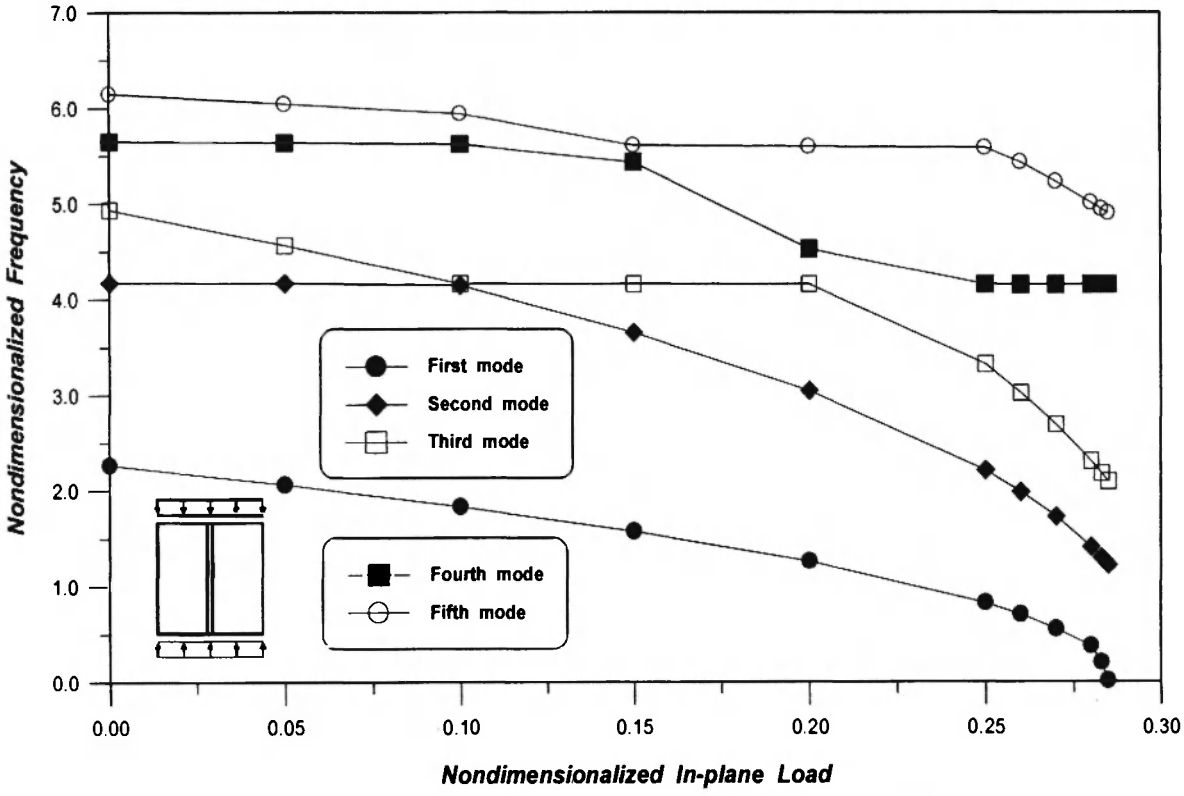

Fig. 15: Non-dimensionalized frequencies of laminated composite stiffened plate under in-plane compressive load

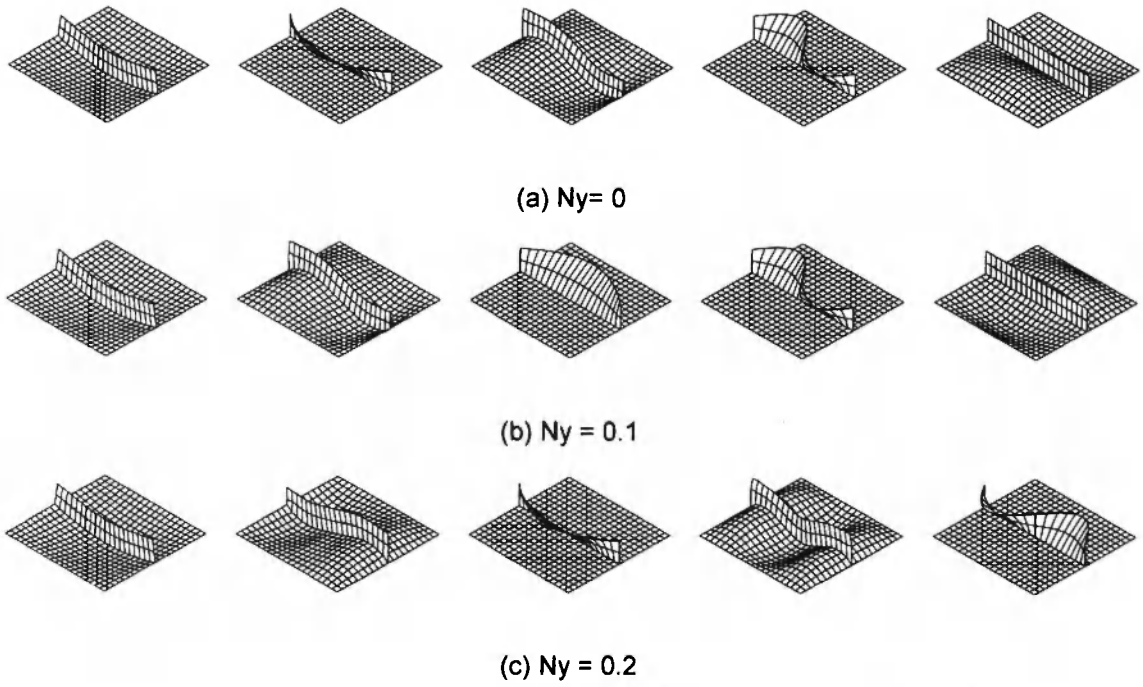

Fig. 16: Mode shapes of stiffened plates under in-plane compressive load

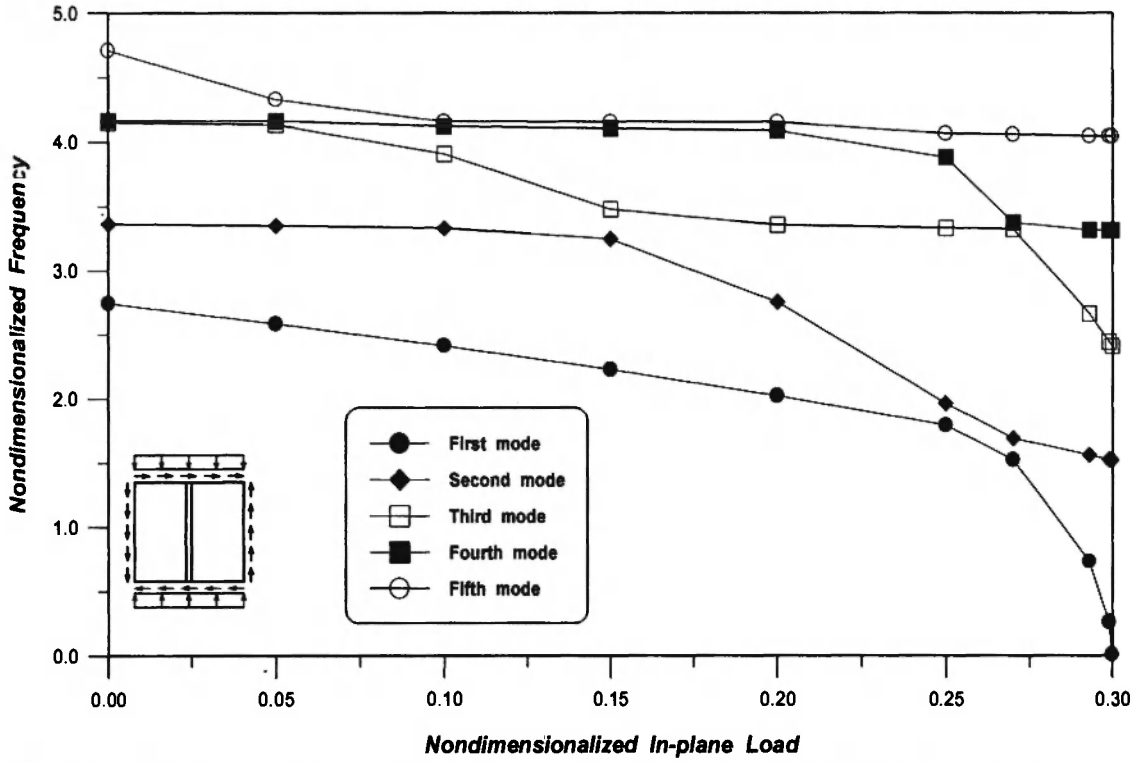

Fig. 17: Non-dimensionalized frequencies of laminated composite stiffened plate under in-plane shear and unidirectional compressive loads $\left(N_{xy} = 0.1\right)$

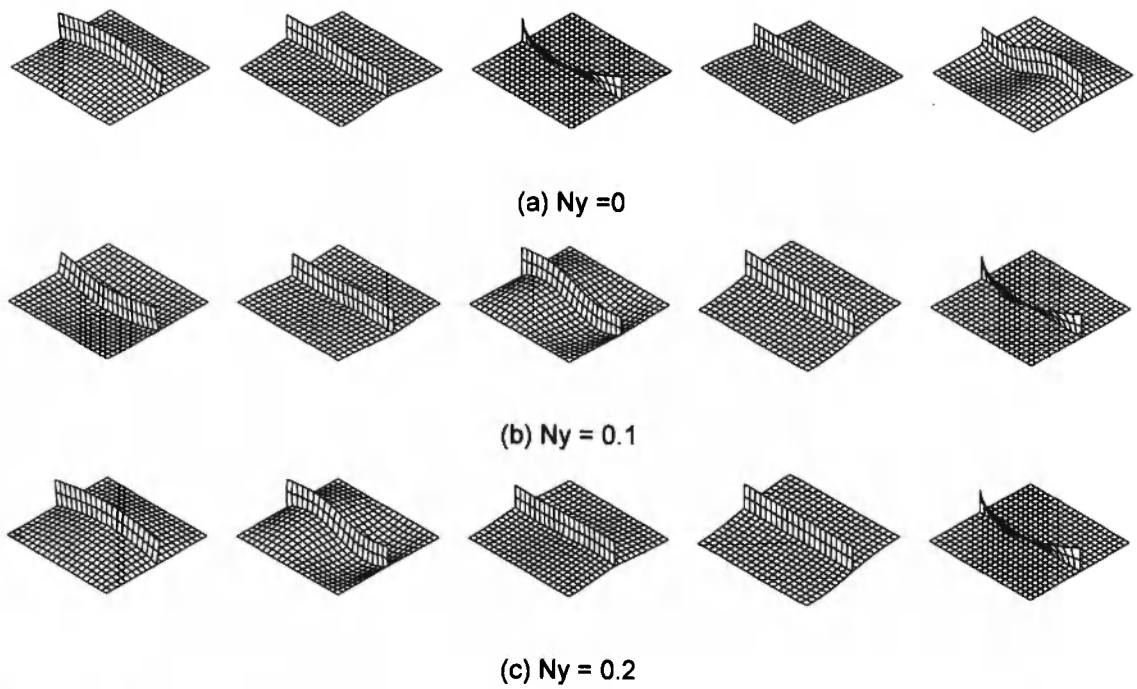

Fig. 18: Mode shapes of stiffened plates under in-plane shear and unidirectional compressive loads $\left(N_{xy} = 0.1\right)$

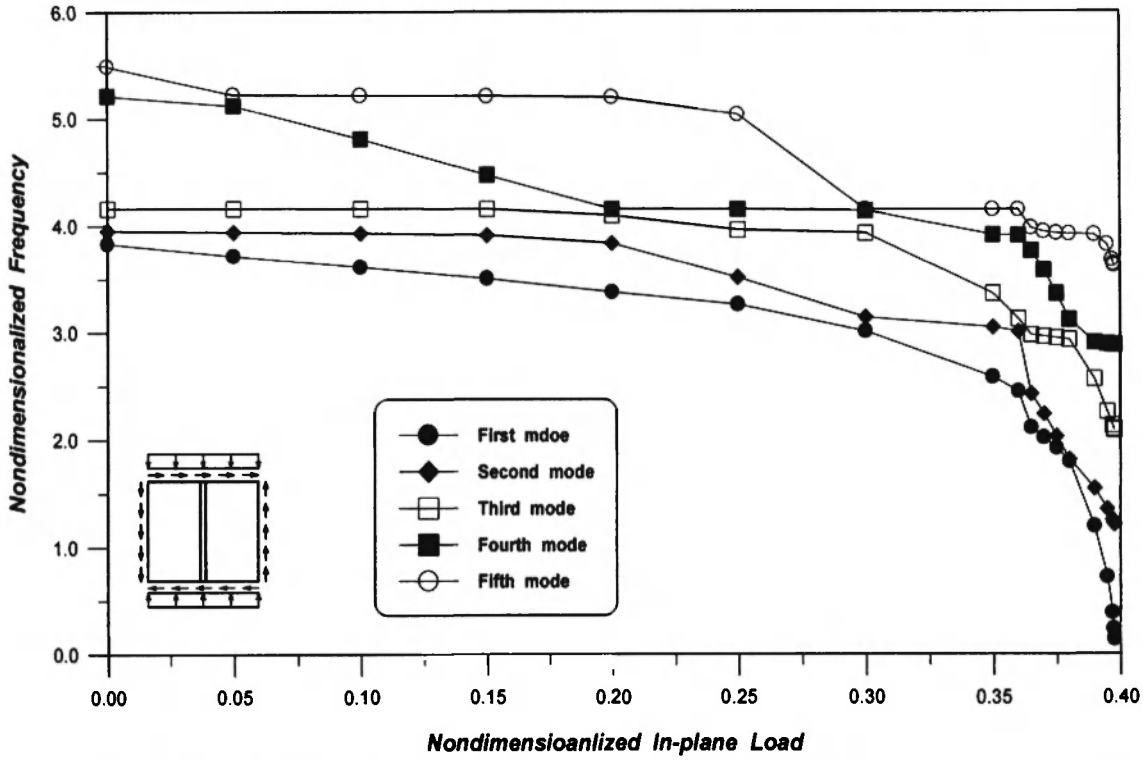

Fig. 19: Non-dimensionalized frequencies of laminated composite stiffened plate under in-plane shear and unidirectional compressive loads $\left(N_{xy} = 0.2\right)$

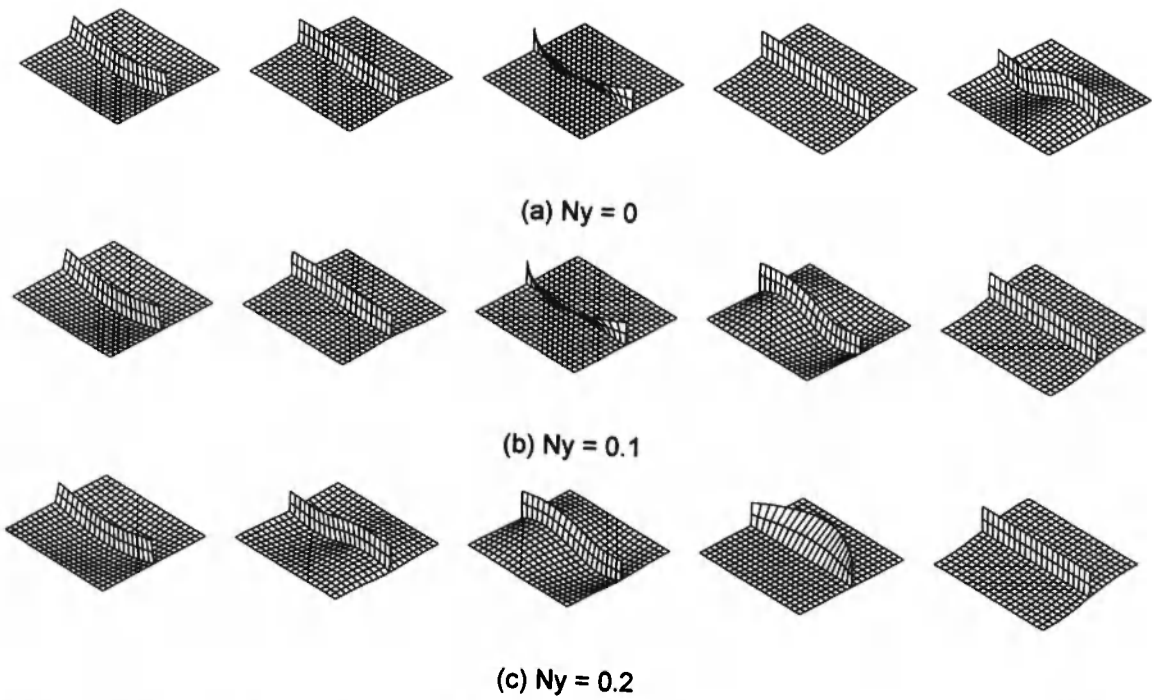

Fig. 20: Mode shapes of stiffened plates under in-plane shear and unidirectional compressive loads $\left(N_{xy} = 0.2\right)$

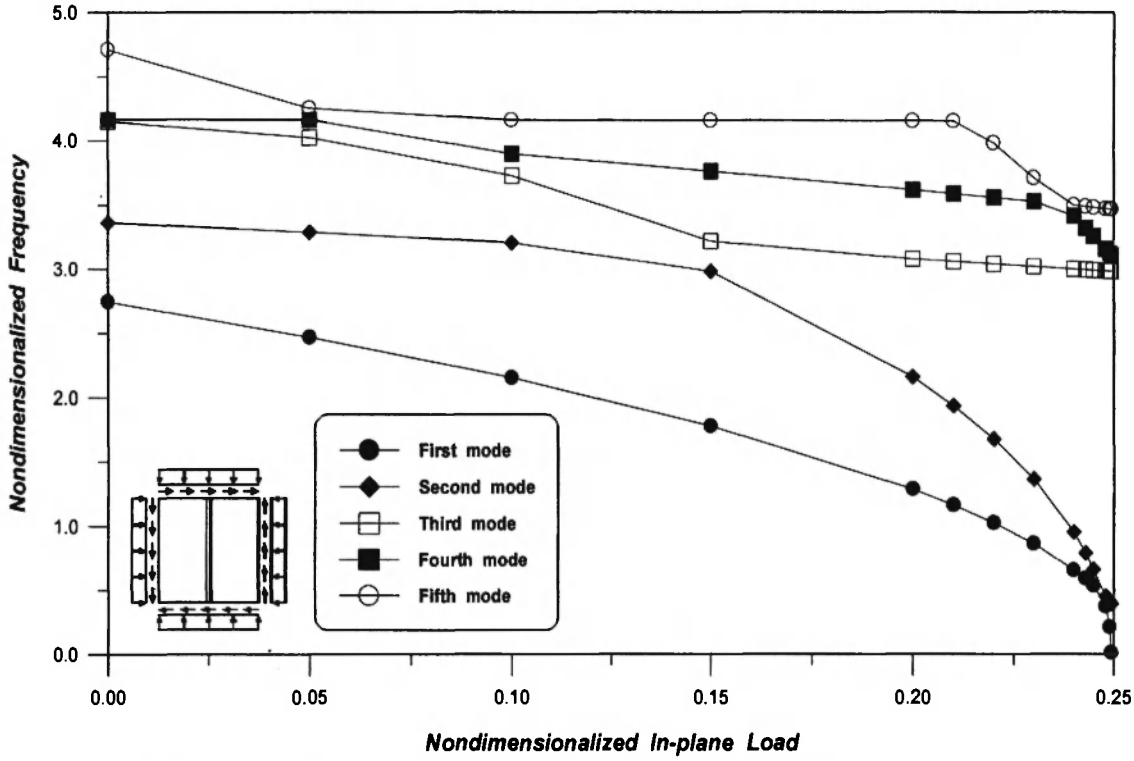

Fig. 21: Non-dimensionalized frequencies of laminated composite stiffened plate under in-plane shear and bidirectional compressive loads $\left(N_{xy} = 0.1\right)$

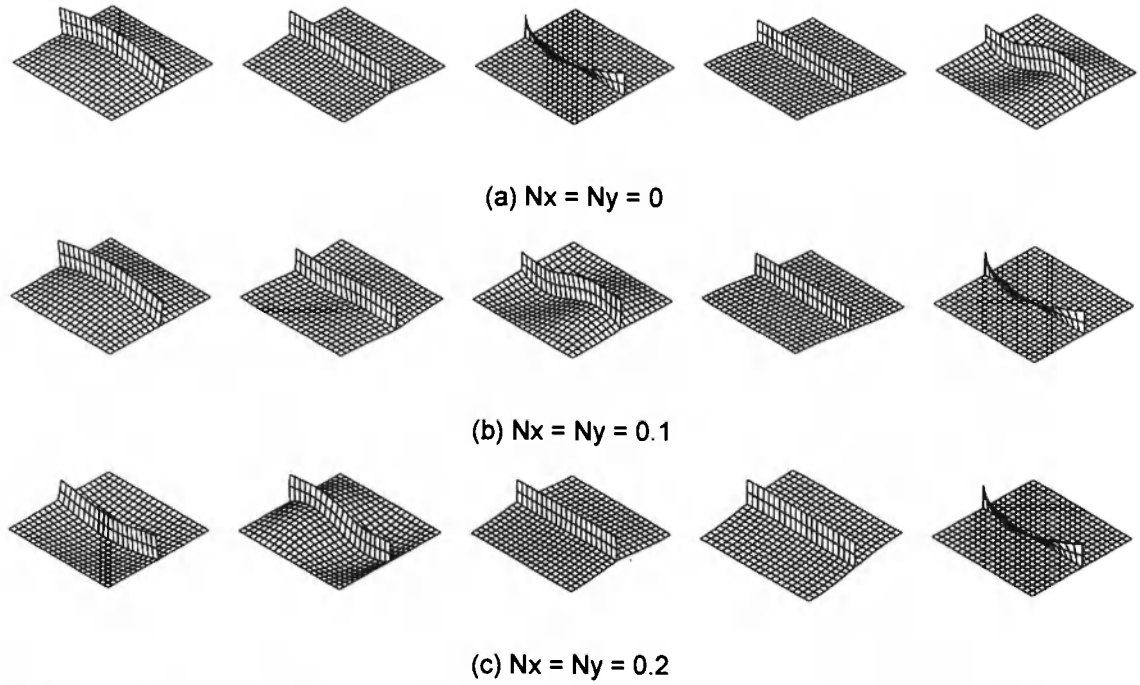

Fig. 22: Mode shapes of stiffened plates under in-plane shear and bidirectional compressive loads $\left(N_{xy} = 0.1\right)$

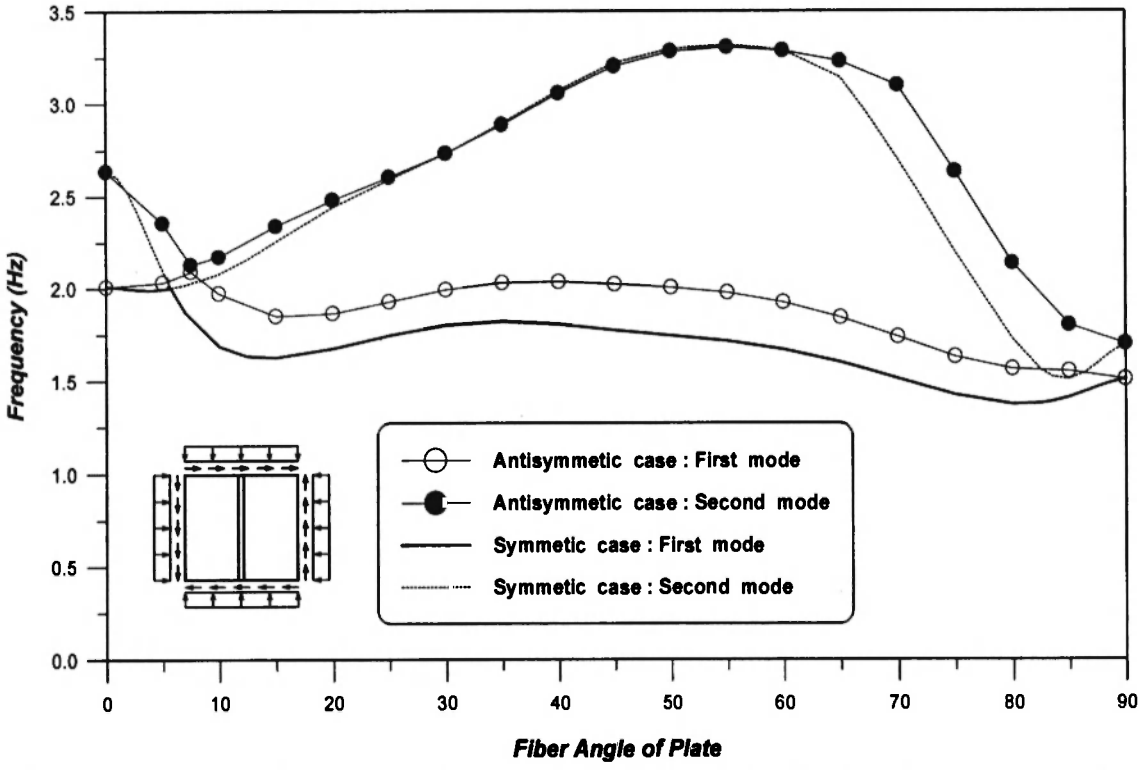

Fig. 23: Non-dimensionalized frequencies of laminated composite stiffened plate under in-plane shear and bidirectional compressive loads

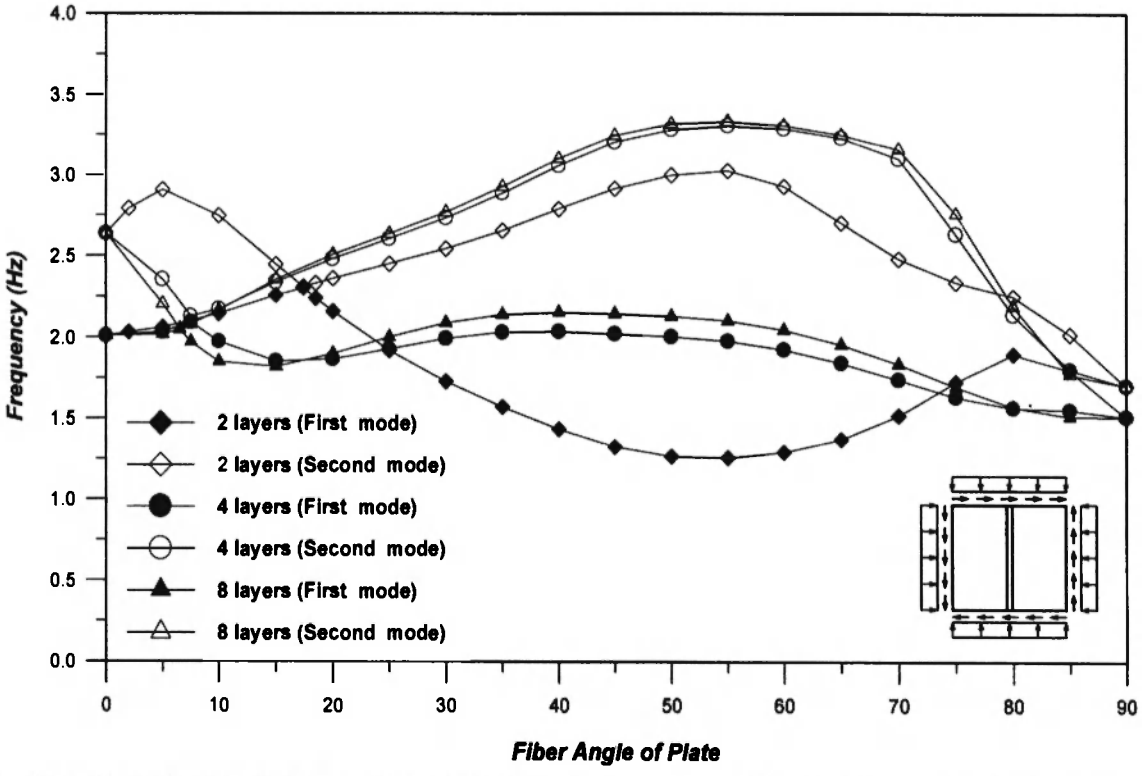

Fig. 24: Non-dimensionalized frequencies of laminated composite stiffened plate under in-plane shear and bidirectional compressive loads

As expected, the intersection, between the curves, interchanges the sequence of some of the mode shapes as a result of the increase in the fiber angle. The intersection point decreases upon increasing the number of layers. The number of layers and fiber angle of skin plate in laminated composite stiffened plates should be selected properly to control the specific frequency and mode shape.

6. CONCLUSIONS

Vibration analysis of laminated composite stiffened plates under the circumstance of combining of in-plane shear and compressive loads is investigated. The 9-node shell element, which is based on assumed strain method and resultant-stress concept, is used. In order to compare with the other references, the vibration analysis of the laminated composite un-stiffened and stiffened plates have been proposed. Natural frequencies for composite stiffened plates obtained from the present analysis are found to be in good agreement with the reference solutions and experiment. In the case of torsionally weak stiffener, a local buckling occurs in the stiffener. In this case, the stiffener should be idealized by using the shell elements. This result shows that the present shell model for the stiffened plate gives more accurate results. The change of stiffener size and location influences the natural frequencies and mode shapes. The fiber orientation of the skin plate affects the natural frequencies of composite stiffened plate more than the fiber orientation of the stiffener.

Relationships between the natural frequencies and the in-plane loads for rectangular composite stiffened plates have been presented. It has been shown that the increase in magnitude of the in-plane compressive load reduces the natural frequencies, which will become zero when the in-plane load is equal to the critical buckling load of the plate. The natural frequencies of composite stiffened plates with shear loads exhibit higher values than the case of without shear loads. The intersection, between the curves of frequencies against in-plane loads, interchanges the sequence of some of the mode shapes as a result of the increase in the in-plane compressive load. Also, the change of direction and magnitude of in-plane load influences the natural frequencies and mode shapes. Besides, the number of layers and fiber angle of skin plate become the reason to change the frequency and the intersection happens in specific fiber angle under the constant in-plane shear and compressive load

Therefore, the magnitude, direction of the in-plane loads, the number of layers and fiber angle of skin plate in laminated composite stiffened plates should be selected properly to control the specific frequency and mode shape.

ACKNOWLEDGEMENTS

The authors would like to express our profound gratitude to Prof. W. Kanok-Nukulchai in AIT, Thailand and Dr. K.D. Kim in Konkuk University, Korea for their encouragement while preparing this paper.

REFERENCES

1. Lee SJ, Han SE. Free-vibration analysis of plates and shells with a nine-node assumed natural degenerated shell element. J Sound Vibr 2001;241:601-633.
2. Reddy JN. Mechanics of Laminated Composite Plates. CRC Press, Florida, 1997.
3. Kant T, Swaminathan K. Analytical solutions for free vibration of laminated composite and sandwich plates based on a higher-order refined theory. Compos Struct 2001;53:73-85.
4. Aydogdu M, Timarci T. Vibration analysis of cross-ply laminated square plates with general boundary conditions. Comp Sci Tech 2003;63(7):1061-1070.

5. Han SC, Choi S. Linear static and free vibration analysis of laminated composite plates and shells using a 9-node shell element with strain interpolation. J. Computational Structural Engineering Institute of Korea 2004;17:279-293. (in Korean)
6. Park TH, Kim KD, Han SC. Linear static and dynamic analysis of laminated composite plates and shells using a 4-node quasi-conforming shell element. Composites Part B: Engineering 2006; 37(2-3):237-248.
7. Kim KD, Liu GZ, Han SC. A resultant 8-node solid-shell element for geometrically nonlinear analysis. Comput Mech 2005;35(5):315-331.
8. Olson MD, Hazell CR. Vibration studies on some integral rib-stiffened plates. J Sound Vibr 1977;50:43-61.
9. Mukherjee A, Mukhopadhyay M. Finite element free vibration of eccentrically stiffened plates. Comput Struct 1988;30(6):1303-1317.
10. Palani GS, Iyer NR, Rao TVSRA. An efficient finite element model for static and vibration analysis of eccentrically stiffened plates-shells. Comput Struct 1992;43(4): 651-661.
11. Liu WH, Chen WC. Vibration analysis of skew cantilever plates with stiffeners. J Sound Vibr 1992;159(1):1-11.
12. Lee DM, Lee I. Vibration analysis of anisotropic plates with eccentric stiffeners. Comput Struct 1995;57(1):99-105.
13. Rikards R, Chate A, Ozolinsh Q. Analysis for buckling and vibrations of composite stiffened shells and plates. Compos Struct 2001;51:361-370.
14. Huang HC, Hinton E. A new nine node degenerated shell element with enhanced membrane and shear interpolation. Int J Num Meth Eng 1986;22:73-92.
15. Jang J, Pinsky PM. An assumed covariant strain based 9-node shell element. Int J Num Meth Eng 1987;24:2389-2411.
16. Simo JC, Hughes TJR. On the variational formulations of assumed strain methods. J Appl Mech ASME 1986;53:51-54.
17. Belytschko T, Wong BL, Stolarski H. Assumed strain stabilization procedure for the 9-node lagrange shell element. Int J Num Meth Eng 1989;28:385-414.
18. Han SC, Kim KD, Kanok-Nukulchai W. An element-based 9-node resultant shell element for large deformation analysis of laminated composite plates and shells. Struct Eng Mech 2004;18(6):807-829.
19. Han SC, Choi S, Chang SY. Nine-node resultant-stress shell element for free vibration and large deflection of composite laminates. J Aero Eng, ASCE 2006;19(2):103-120.
20. Han SC, Lee SY, Rus G. Postbuckling analysis of laminated composite plates subjected to the combination of in-plane shear, compression and lateral loading. Int J Solids Struct 2006; 43(18-19):5713-5735.
21. Lee WH, Han SC. Free and forced vibration analysis of laminated composite plates and shells using a 9-node assumed strain shell element. Comput Mech 2006; 39(1):41-58.
22. Kim KD, Lomboy GR, Han SC. A co-rotational 8-node assumed strain shell element for postbuckling analysis of laminated composite plates and shells. Comput Mech 2003;30(4):330-342.
23. Attaf B, Hollaway L. Vibrational analyses of stiffened and unstiffened composite plates subjected to in-plane loads. Composites 1990;21(2):117-126.
24. Groesberg SW. Advanced Mechanics. Wiley, New York, 1968.
25. Whitney JM. Shear correction factors for orthotropic laminates under static loading. J Appl Mech ASME 1973;40:302-304.
26. Kanok-Nukulchai W. A simple and efficient finite element for general shell analysis. Int J Num Meth Eng 1979;14:179-200.